Geo-Mar Lett (2014) 34:525–540
DOI 10.1007/s00367-014-0383-1

ORIGINAL

A new pathway for Deep water exchange between the Natal Valley and Mozambique Basin?

Errol Wiles · Andrew Green · Mike Watkeys · Wilfried Jokat · Ralf Krocker

Received: 8 July 2014 / Accepted: 2 September 2014 / Published online: 27 September 2014

Abstract Although global thermohaline circulation pathways are fairly well known, the same cannot be said for local circulation pathways. Within the southwest Indian Ocean specifically there is little consensus regarding the finer point of thermohaline circulation. We present recently collected multibeam bathymetry and PARASOUND data from the northern Natal Valley and Mozambique Ridge, southwest Indian Ocean. These data show the Ariel Graben, a prominent feature in this region, creates a deep saddle across the Mozambique Ridge at ca. 28°S connecting the northern Natal Valley with the Mozambique Basin. Results show a west to east change in bathymetric and echo character across the northern flank of the Ariel Graben. Whereby eroded plastered sediment drifts in the west give way to aggrading plastered sediment drift in the midgraben, terminating in a field of seafloor undulations in the east. In contrast, the southern flank of the Ariel Graben exhibits an overall rugged character with sediments ponding in bathymetric depressions in between rugged sub/outcrop. It is postulated that this change in seafloor character is the manifestation of deep water flow through the Ariel Graben. Current flow stripping, due to increased curvature of the graben axis, results in preferential deposition of suspended load in an area of limited accommodation space consequently developing an over-steepened plastered drift. These deposited sediments overcome the necessary shear stresses, resulting in soft sediment deformation in the form of down-slope growth faulting (creep) and generation of undulating sea-floor morphology. Contrary to previous views, our works suggests that water flows from west to east across the Mozambique Ridge via the Ariel Graben.

E. Wiles (✉) · A. Green · M. Watkeys
Geological Sciences, School of Agricultural, Earth and Environmental Sciences, University of KwaZulu-Natal, Private Bag X 54001, Durban 4000, South Africa
e-mail: eawiles@yahoo.com

W. Jokat · R. Krocker
Alfred-Wegener-Institute for Polar and Marine Research, Am Alten Hafen 26, Bremerhaven 27568, Germany

Introduction

The global transfer of heat and nutrients is driven by thermohaline circulation (THC) within the ocean basins. The THC system comprises a network of bottom, deep and surface currents that conserve mass and energy in the World's oceans by the creation of a complex system of circulation cells. The southwest Indian Ocean (SWIO) is a dynamic region of ocean exchange between the Indian, Atlantic and Southern Oceans representing a pivotal component of the THC system. In general, both bottom and deep water circulation pathways around the globe and within the SWIO are well known and constrained. The residence times of these deep and bottom waters have significant implications for long-term climate state as well as CO_2 sequestration (Martin 1981a; Martin 1981b; Ben-Avraham et al. 1994; Srinivasan et al. 2009). As a result, the greater THC system has garnered increased attention over the past two decades, particularly in light of their potential roles driving both palaeo and future climate change (Martin 1981a; Martin 1981b; Raymo et al. 1990; Winter and Martin 1990; Raymo et al. 1997; Schmieder et al. 2000; Srinivasan et al. 2009; Gutjahr et al. 2010). However, at a more localised scale, THC pathways are often poorly constrained. Many factors, including the Earth's rotation (Coriolis Effect), ocean basin macrotopography, ocean gateways, prevailing winds, and glacial/ inter-glacial cycles have a direct impact on THC circulation and transport volumes. This research examines deep water bottom currents in the context of seafloor macrotopography and interprets these in light of several possible deep water circulation systems in the Natal Valley, SWIO.

Since the initial research thrust in the Natal Valley (cf. Martin 1981a; Martin 1981b; Dingle et al. 1978; Dingle et al. 1987,

Winter and Martin 1990), little additional research associated with the Natal Valley has been undertaken; this is especially true for the deep, northern portions of the Natal Valley. Notable exceptions include studies on the interactions between bottom water currents (those deep currents in contact with the seafloor) and sediments from the Natal Valley (Niemi et al. 2000; Wiles et al. 2013), and submarine canyons of the upper slope (Green et al. 2007; Green and Uken 2008; Green 2011a).

This paper presents a new, higher resolution dataset of the area, highlighting several key seafloor and subsurface features that reveal a potential new deep water pathway across the Mozambique Ridge (via the Ariel Graben) to the Mozambique Basin, as described by new multibeam bathymetry and high frequency seismic data from the Natal Valley, SWIO. The aim of this paper is to reconcile this with the major THC systems in the area.

Physical setting

Geology and physiography

Bound to the west by the south-east African continental margin and to the east by the Mozambique Ridge, the Natal Valley is a north–south orientated basin located in the SWIO (Fig. 1). To the south the Natal Valley merges (below 4000 m) with the Transkei Basin. Shoaling northward, the Natal Valley extends toward the extensive low-lying coastal plains of southern Mozambique (Dingle et al. 1978; Goodlad 1986). The Natal Valley, divided in to a northern and southern portion at 30°S, is the product of two distinct spreading centres. The northern portion of the basin opened ca. 183–158 Ma (Leinweber and Jokat 2011), while the southern portion was the result of spreading from 138.9–130.3 Ma (Leinweber and Jokat 2012). The basin was fully developed by 90 Ma (Martin and Hartnady 1986; Ben-Avraham et al. 1994).

The western margin of the Natal Valley exhibits an anomalously narrow, 4–15 km wide, coast-parallel shelf (Dingle and Robson 1985; Green 2011a; Green 2011b; Cawthra et al. 2012). Departure from the narrow shelf is observed offshore of the Limpopo and Thukela rivers where sediment cones prograde into the Natal Valley (Dingle et al. 1978; Martin 1981a; Martin 1981b; Martin 1987). Over the past 65 Ma, sediment input into the Natal Valley has been estimated at ca. 23 $m^3/km^2/yr$; the Limpopo and Thukela rivers delivering the bulk of sediment to the basin, amounting to the deposition of an 800 m thick layer of sediment within the basin (Flemming 1980). Oligocene to present day sedimentation is characterised by erosion and redistribution throughout the Natal Valley and Transkei Basin (Martin 1981a; Martin 1981b; Niemi et al. 2000).

Bathymetric features pertinent to this study are the Central Terrace, Naudé Ridge, Mozambique Ridge (Dana Plateau in particular), Ariel Graben, Tugela cone and Limpopo cone (Fig. 1). The Central Terrace is a north–south orientated

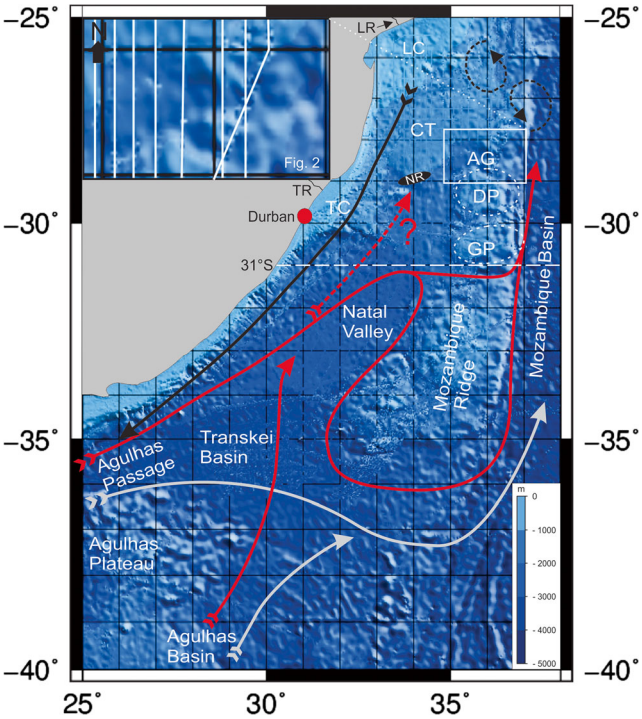

Fig. 1 The general bathymetry (The GEBCO_08 Grid, version 20091120) of the southwest Indian Ocean (modified after Wiles et al. 2013). Presently known THC pathways are shown; black arrow illustrates the Agulhas Current, red—the North Atlantic Deep Water, and grey—the Antarctic Bottom Water (after Bang and Pearce 1976; Casal et al. 2006; Dingle et al. 1987; Toole and Warren 1993; Schlüter and Uenzelmann-Neben 2008; van Aken et al. 2004). Eddies associated with the Mozambique and East Madagascar Currents are shown by dashed circular arrows (Quartly and Srokosz 2004). The Tugela Cone (TC), Limpopo Cone (LC) and Central Terrace (CT) are located west of the study area (white box), which is enlarged to show the ship tracks. The Dana (DP) and Galathea Plateaus (GP) of the northern Mozambique Ridge are indicated by dashed circles. North of the Dana Plateau lies the Ariel Graben (AG), a west/east saddle across the Mozambique Ridge The most prominent rivers flowing in to this Natal Valley region are the Thukela River (TR) in South Africa, and the Limpopo River (LR) in Mozambique. The Naudé Ridge (NR) is a buried basement high. A more detailed overview of the study area is provided in Fig. 2

basement high that provides the northern bathymetric depth constraint within the northern Natal Valley (Figs. 1 and 2). The Central Terrace has a smooth convex surface flanked to the east and west by prominent valleys, whereas the southern flank comprises a steep, smooth slope that extends down to the deep central northern Natal Valley (Dingle et al. 1978). The steep southern slope is the topographic expression of the Naudé Ridge, a prominent basement high now overlain by sediment (thickness of 1 s TTWT) (Dingle et al. 1978). The Tugela and Limpopo cones represent fan shaped features prograding into the Natal Valley from offshore of the Thukela and Limpopo rivers respectively (Fig. 1). The Tugela cone exhibits a steep, west to east southern flank, while the eastern flank has a more moderate gradient and hummocky surface. Numerous terraces create complex bathymetry over the surface of the cone, which is crosscut by the Tugela canyon

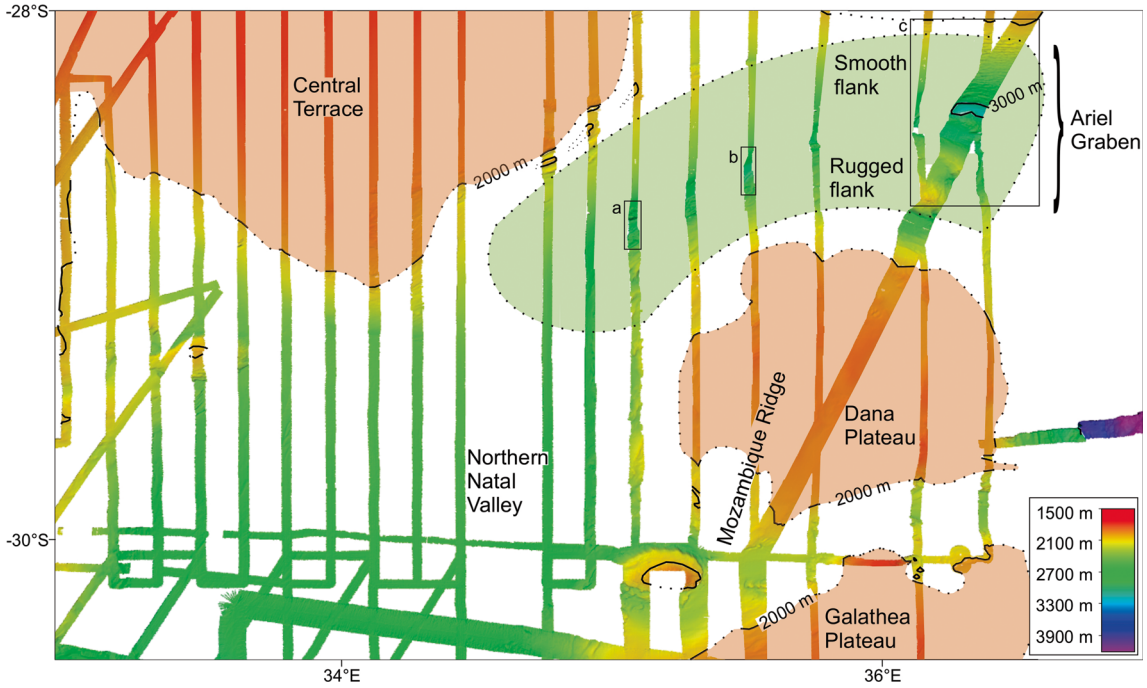

Fig. 2 An overview of the northern Natal Valley and northern Mozambique Ridge. Note the 2000 m isobaths to the NW (Central Terrace) and SE (Dana Plateau), as well as the saddle created by the Ariel Graben. Boxes *a*, *b*, and *c* show areas enlarged in Figs. 3, 4, 5 and 6, and are referred to in text

(Dingle et al. 1978). The Pleistocene age Tugela canyon delivers what little sediment crosses the sediment starved shelf to the Tugela fan which has been winnowed and modified by sweeping of the NADW (Wiles et al. 2013). The Limpopo cone lies north of the Tugela cone, and northwest of the Central Terrace, extending 300 km south of the Limpopo River (Martin 1981a). This sedimentary cone is separated from the continental shelf of southern Mozambique by a narrow valley, similar to that of the Central Terrace to the southeast (Dingle et al. 1978). To the east of the Natal Valley the north/south orientated Mozambique Ridge provides further bathymetric constraint in the form of numerous submarine plateaus. Of importance in this study are the northern Dana and Galathea plateaus (Fig. 1). The northern Dana Plateau is the larger or the two, measuring 120×130 km in dimension, and rising to a depth of 1795 m below the sea surface. The northern flanks of the Dana Plateau deepen into the Ariel Graben (comprising the southern flank of the Ariel Graben), a west/east orientated 12 km wide saddle that crosses the Mozambique Ridge at 28°30'S (Figs. 1 and 2). South of the Dana Plateau the Galathea Plateau rises to shallower depths (1600 m) extending 150 km in an east/west orientation, and 80 km north/south.

Current state of knowledge regarding circulation in the Natal Valley

Circulation within the Natal Valley, and surrounding SWIO, is complex owing to the macrotopography of the basins and the adjacent narrow continental shelf (Fig. 1). Two main circulation systems are recognised, The Agulhas Current and the North Atlantic Deep Water (NADW).

The Agulhas Current is a fast (4 knots), poleward flowing, wide (ca. 100 km) geostrophic current that dominates the upper ocean flow along the western boundary of the Natal Valley (Bang and Pearce 1976; Dingle et al. 1987, Martin 1981a; Martin 1981b; Donohue and Toole 2003; Lutjeharms 2007, McDonagh et al. 2008) (Fig. 1). The precise source area for the Agulhas Current is unknown; however sedimentological studies suggest this source area lies between 26°S and 30°S offshore the east African coast (Flemming 1980; Martin 1981a; Martin 1981b; Lutjeharms 2006a, 2006b). This is a dynamic region influenced by several water masses. Southward flowing eddies from the Mozambique Channel meet with eddies of the East Madagascar Current, with additional input from the Agulhas Return Current (Stramma and Lutjeharms 1997; de Ruijter et al. 2003; Quartly and Srokosz 2004; Quartly and Srokosz 2004; Lutjeharms 2007). A deep-reaching current, the Agulhas Current is considered by some to progressively extend to depths of as much as 2500 m by 32°S along South Africa's southeast coast (Bang and Pearce 1976; Pearce 1977; Dingle et al. 1987; Beal and Bryden 1999; Donohue and Toole 2003). However, in some instances it has only been the upper 500 m of the Agulhas Current that was intensely studied (Pearce 1977), whereas the structure below 1000 m was estimated or shown to be shallower than the sea bottom (Donohue et al. 2000). As such a complete understanding of the variability of depth changes and the

influencing factors of the Agulhas Current remains elusive (Lutjeharms 2006a).

The northern section of the current system is remarkably stable, owing to the steep, linear continental shelf of northern South African margin that steers the current flow (de Ruijter et al. 1999; Lutjeharms 2006a; Lutjeharms 2007). A consequence of this stable linear flow path is that the southward flow associated with the Agulhas Current terminates ca. 200 km offshore (Lutjeharms 2006b). Inshore of this northern Agulhas Current, Beal and Bryden (1997) describe an undercurrent at ca. 31°S flowing northward along the continental slope at 1200 m depth, and directly beneath the surface core of the Agulhas Current. Numerical models have produced comparable flows at ca. 34°S, with the depth of the undercurrent varying from 300–2500 m (see Lutjeharms 2006a).

Other authors consider the bottom water circulation within the Natal Valley to be governed by the northeasterly flowing NADW, a deep western boundary current. Two possibly contemporaneous pathways have been proposed to describe the passage of NADW (ca. $1.2x10^6$ $ms^{-1)}$ into the Natal Valley (Fig. 1). The first (southern) pathway is facilitated by the South Atlantic Current. This pathway is envisaged as transporting NADW around the southern tip of Africa. The NADW core then bifurcates; the northern branch (confined to a depth of 2000–3500 m, and salinity of 34.83 %) continuing northeastward, via the Agulhas and Transkei basins, into the Natal Valley. In contrast, the southern branch of NADW continues eastward beneath the meandering Agulhas Return Current and does not enter the Natal Valley (Toole and Warren 1993; van Aken et al. 2004).

The second (northern) NADW pathway is considered to flow along the African continental slope at depths between 2000 and 2500 m. This NADW core passes, via the Agulhas Passage, into the Transkei Basin on its pathway into the Natal Valley (Toole and Warren 1993; van Aken et al. 2004; Schlüter and Uenzelmann-Neben 2008). Confined by shoaling bathymetry within the Natal Valley, the NADW is believed to return southward along the eastern boundary of the Natal Valley (constrained by the western slopes of the Mozambique Ridge) (Dingle et al. 1987; McDonagh et al. 2008). Van Aken et al. (2004) considered some leakage across a saddle in the Mozambique Ridge at ca. 31°S and at depths of 2500–3000 m.

Within the southern Natal Valley a net northeastward flow of NADW, west of 32°E was confirmed (Beal and Bryden 1999; Donohue et al. 2000; Donohue and Toole 2003, McDonagh et al. 2008). It is this deep northward flow of the NADW which is likely responsible for winnowing of the Tugela fan in the mid-western Natal Valley (Wiles et al. 2013).

Further north, hydrographic observations from the Mozambique Channel showed a variable northward flowing undercurrent along the western channel at 1500–2400 m depth, inshore of the southward migrating Mozambique Current eddies (de Ruijter et al. 2002; DiMarco et al. 2002; Ullgren et al. 2012). The deep core of this undercurrent comprises NADW (flowing at $4x10^6 m^3 s^{-1}$) which, at 2000 m, is able to cross the shallowing sill of the Mozambique Channel (2500 m) and continue into the Somali Basin (Donohue and Toole 2003; van Aken et al. 2004). The NADW that does not cross this sill is considered to return southward along the eastern side of the Mozambique Channel and Basin (Donohue and Toole 2003).

Seafloor/current interactions

In the northernmost and shallowest portions of the Natal Valley, seafloor/current interactions were recorded as areas of non-deposition on the Limpopo Cone and Central Terrace (Martin 1981a, 1981b; Preu et al. 2011). This interaction between the Agulhas Current and the northernmost Natal Valley has a minimum age of Early/Middle Miocene (Martin 1981a; Preu et al. 2011). Although initially variable, the Agulhas Current pathways were thus fairly stable following the Early Miocene. Erosion and redistribution of sediment on the Limpopo cone and Central Terrace, between depths of 400–1500 m, can therefore be attributed to the net southward flow of the Agulhas Current.

Deeper into the Natal Valley (ca. 2500–3000 m) and further south (ca. 33°S), Dingle et al. (1987) recognise recirculation of NADW within the Natal Valley based on the location, orientation, depth and character of sediment drifts in the basin. Through interactions with the seafloor sediments, the NADW has developed two elongate, north/south orientated, sediment drifts. The western drift and eastern drift associated with northward and southward flow respectively since the Late Eocene (Dingle et al. 1987).

Material and methods

A portion of data from two recent research cruises, AISTEK II (20th of May-7th of July, 2005) aboard the R/V Sonne (Jokat 2006) and AISTEK III (9th of April-1st June, 2009) aboard the R/V Pelagia (Jokat 2009), are used in this study. AISTEK II investigated the Mozambique Basin and Ridge using a SIMRAD EM120 multibeam echosounder. A Kongsberg EM300 multibeam echosounder was used to acquire bathymetry data over the Mozambique Ridge and Natal Valley during the AISTEK III survey. Both multibeam data sets were processed onboard using CARIS HIPS and exported as xyz ASCII

files. Interactive Visualization Systems' DMagic (version 7.3.1a) was used to grid the data, which were then displayed in Fledermaus (version 7.3.1a) for interpretation. The final bathymetry data have an output matrix of ~35 m, providing a relatively high resolution dataset. Specific portions of these data are presented in this study to illustrate the results and discussion graphically.

A 3.5 kHz (AISTEK III) and a parametric ATLAS PARASOUND echosounder (AISTEK II) were used to collect seafloor and sub-bottom data during the respective cruises. These data sets provide very high frequency seismic data with a vertical resolution ca. 1 m. Due to technical difficulties, complete seismic coverage along track was in some instances not achievable. In-house designed software, in addition to SEISEE (version 2.17.1.), were used to process the data. These data were incorporated into SEISEE for visualization and interpretation of the echo character. Band pass filter adjustments and colour gains were applied to the data.

Results

A wide, channel-like feature is evident in the multibeam bathymetric data, leading from the mid-Natal Valley across the Mozambique Ridge toward the Mozambique Basin (Fig. 2). Confined to the north–west by the Central Terrace, and the south–east by the Dana Plateau (Mozambique Ridge), the channel is located in the bathymetric depression associated with the Ariel Graben (Fig. 2). Rugged bathymetry is more common on the northern flanks of the Dana Plateau (i.e., southern flank of the Ariel Graben) than on the Central Terrace, where seafloor is smooth (Fig. 2). This rugged bathymetry is confined to depths of 2000–3000 m on the northern flank of the Dana Plateau where there is a significant amount of basement control on topography. Evidence of this is manifest in the highly irregular, rugged bathymetry, and seismic character presented in Figs. 3 and 4. Although the Ariel Graben has created an overall west to east orientated saddle, the actual depression follows a curved path (Fig. 2). The degree of change in channel axis orientation increases more rapidly in the west in the vicinity of box c (Fig. 2).

Boxes a and b (Fig. 2.) are enlarged in Figs. 3 and 4 respectively. These figures illustrate in detail the bathymetry and shallow seismic character of this portion of the Mozambique Ridge. The northern flanks of the channel return distinct bottom echoes, with several discontinuous sub-bottom echoes (profile A—A' in Fig. 3, and profile B—B' in Fig. 4). The seafloor is smooth, with no apparent basement outcrop or subcrop visible within the limit of penetration (20 m) and coverage. The gradient of the northern flank is variable, (0.3°–2.1°, total slope average is 1°), typically increasing with depth (north to south toward the channel) to a maximum of 5.7° nearest the channel. Steepest gradients (5°–6°) are noted in the central region of the saddle across the Mozambique Ridge (Figs. 3 and 4).

The channel floor ranges in width from 4385 m to 5100 m with a variable echo character. In the western portions of the channel, hyperbolic reflectors are evident in the 3.5 kHz profile (profile A—A' in Fig. 3). The hyperbolae are of a similar height above the seafloor, and vary from individual to overlapping in organisation. Bathymetric data show this area to be rough / undulating. Smooth seafloor in the bathymetry is associated with distinct seafloor returns and continuous and sub-parallel sub-bottom reflector packages (profile B—B' in Fig. 4). An elongate terrace, orientated parallel to the base of the southern flank, is evident in both the bathymetry and shallow seismic data suggesting some degree of lateral and vertical erosion (profile B—B' in Fig. 4).

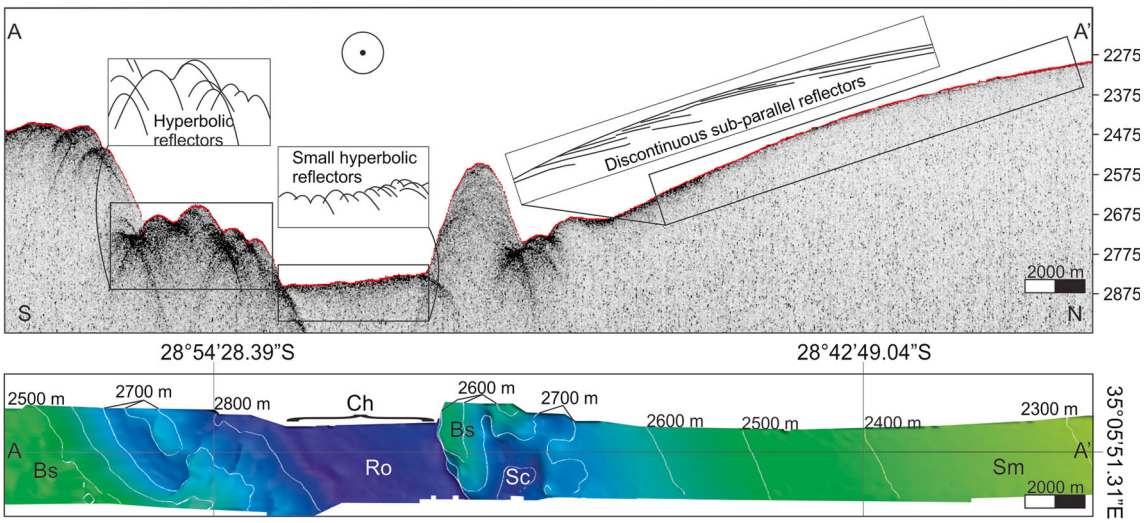

Fig. 3 Enlarged bathymetry of box a in Fig. 2. The contrast between the smooth seafloor (Sm) of the northern flank and the rugged seafloor (Bs), reflecting some basement control, of the southern flank is evident in the multibeam bathymetry (*bottom*) and high frequency seismic record (profile A—A', *top*). Note the apparent scouring (Sc) around basement outcrop in the saddle floor

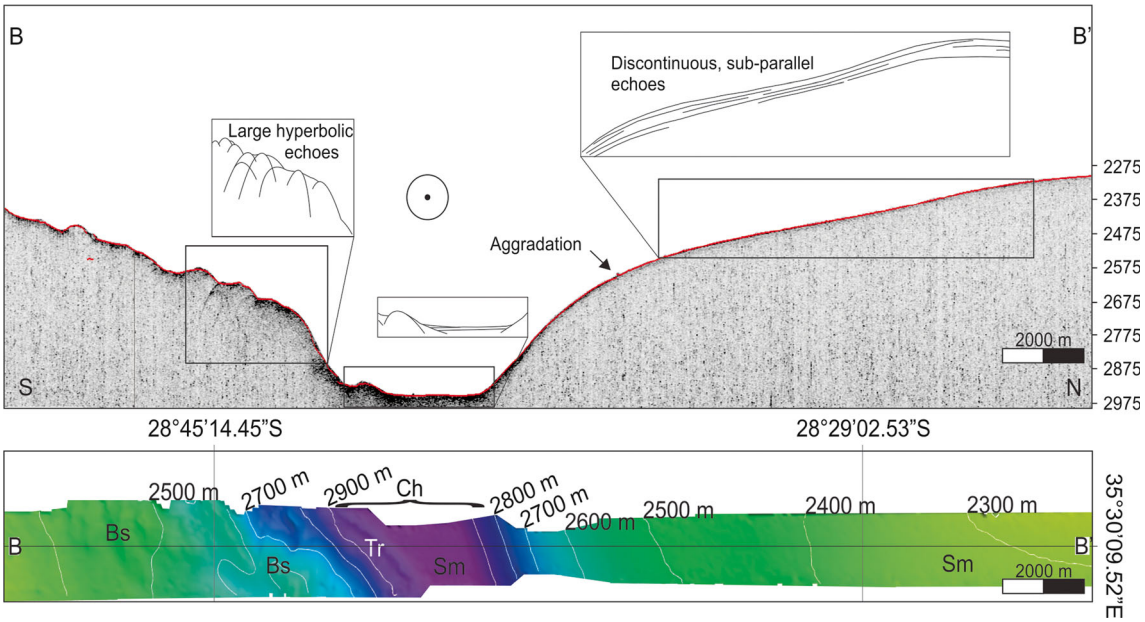

Fig. 4 Enlarged bathymetry of box b in Fig. 2. The contrast between the smooth seafloor (Sm) of the northern flank and the rugged seafloor (Bs) of the southern flank of the Ariel Graben is clear in the multibeam bathymetry (*bottom*) and high frequency seismic record (profile B—B', *top*). Note the change in character of the floor of the saddle. A terrace (Tr) is apparent at the base of the southern flank

The southern flanks of the channel are distinct from the northern flanks in both bathymetric and seismic character. Large, irregular, hyperbolae, ranging in size, amplitude and spacing (over-lapping to 1 km) dominate the seismic profiles (Figs. 3 and 4). Intense overlapping is focused on the more rugged areas, while individual hyperbolae are observed where the bathymetry is less complex. Rugged bathymetry associated with such echoes, exhibit highly variable gradients (0.3°–19.6°). Overall, the channel floor is relatively flat, while the profile of the channel is "U"-shaped. Scouring has modified this "U" shape in certain areas of the lower channel flanks suggesting sustained reworking and removal of sediment (Fig. 3).

There is a notable eastward change in character of the seafloor on the northern flanks of the channel (Fig. 5). At depths between 2100 m and 3000 m, the seafloor displays an undulating morphology (Fig. 5 and profile C—C' in Fig. 6). These undulations are straight crested and parallel/sub-parallel to the local isobaths, with crest long axes orientated west to east. Spacing between the crests is variable. The middle zone (2330–2677 m) is typified by undulations with 600–900 m wavelengths, whereas the upper and lower zones have distances of 1000–1200 m between crests. Cross- sectional symmetry of these features varies from symmetrical to asymmetrical, with broad crests and narrow troughs (Fig. 5). When asymmetrical, the down-slope (south-facing) limb is longer (511.76 m average) than the up-slope (north-facing) limb (323.53 m average) (Table 1). The lower limbs are also steeper than the upper limbs; calculated averages being 3.80° and 1.55°, respectively (Table 1). Overall the total slope on which the undulations are found is south-facing with a gradient of 1.54°, however, the area affected by undulations is slightly steeper with an average slope of 1.75°. Beyond 3000 m (the lower limit of the undulations), the gradient increases to 4.71° at the flank/channel floor transition. North of the undulations (above 2100 m) the seafloor becomes smooth once more, reflecting similar characteristics to that of the western portion of the study area (Fig. 5 and profile D—D' in Fig. 6). The total slope average in this eastern region is 0.54°, thus steeper than to the west. The channel floor, no longer flat, is ca. 440 m wide at 3160 m depth. The profile now has a more "V"-shaped section.

The southern flank of the channel is more rugged than the northern flank (Fig. 5). Hyperbolic echoes (from the 3.5 kHz echo trace) are associated with rugged bathymetry (profile E—E' in Fig. 6). Distinct bottom echoes, with several sub-parallel sub-bottom reflector packages are noted in areas of flat lying bathymetry (profile E—E' in Fig. 6). These packages onlap the rugged subcrop, showing varied package thickness and amplitude. The lowermost packages comprise low amplitude, transparent packages that thicken from south to north, while toward the seafloor surface, high amplitude packages of uniform thickness are evident. The gradient of the southern flank is highly variable, reaching a maximum of 10.5° in the rugged areas, whereas areas of subdued bathymetry exhibit low gradients (0.18°). The total gradient is 1.34° but is a poor indicator of the seafloor character due to marked variability in the gradient of the area (Fig. 7). The variation of the rugged southern flank is far greater and widespread than that of the north (Fig. 7). Only in the eastern portions of the study area, on the northern flank, does the gradient begin to vary as the undulation field is encountered (Fig. 7).

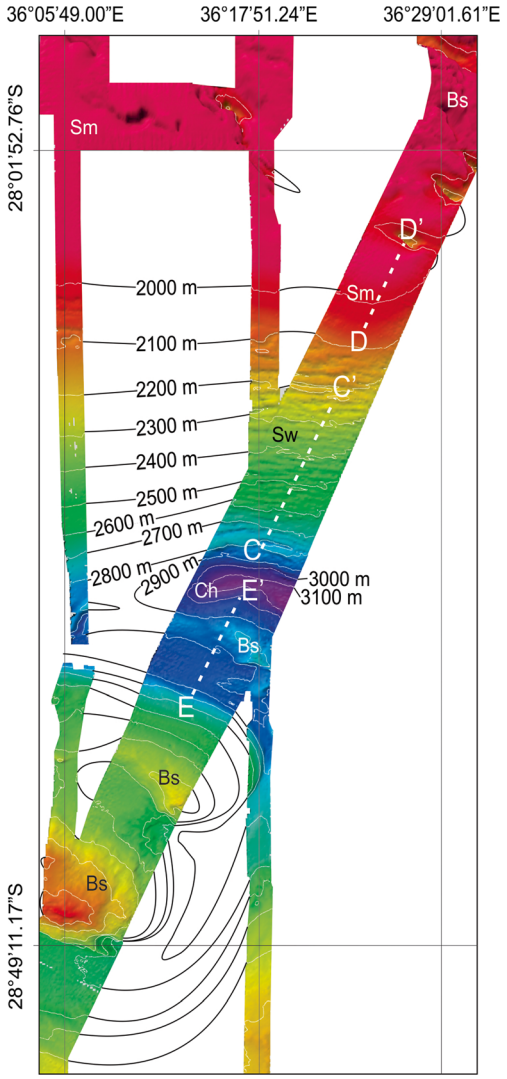

Fig. 5 The eastern region of the Ariel Graben revealed in the multibeam data (See Fig. 2, Box c for location). Note elements of basement control (Bs), smooth seafloor (Sm), and undulation field (Sw). The channel floor (Ch) is now narrower than in the west toward the Natal Valley. Profiles C—C', D—D', and E—E' shown in Fig. 6

Discussion

Echo character contrasts

There is distinct contrast in the echo character of the Ariel Graben's northern and southern flanks. The northern flank (western area) shows distinct, high amplitude, bottom echoes with several discontinuous parallel/sub-parallel sub-bottom reflectors. This echo character is synonymous with the development of crude plastered drifts, as described from other regions (cf. Damuth 1975; Damuth 1980; Jacobi 1982; Faugères et al. 1999; Stow and Mayall 2000; Masson et al. 2002; Maldonado et al. 2003; Stow et al. 1996), and the same deposit is envisioned in this study (Figs. 3, 4 and 6). This is further demonstrated by the areas of smooth seafloor (Sm in Figs. 3, 4 and 5) where current-plastering has created a uniform surface relief. This seafloor character has similar associations to plastered drifts, discussed from other regions by multiple authors (Damuth 1975; Damuth 1980; Jacobi 1982; Faugères et al. 1999; Stow and Mayall 2000; Masson et al. 2002; Maldonado et al. 2003; Stow et al. 1996). Along the northern flanks of the eastern Ariel Graben, seafloor undulations (Fig. 5) are associated with large, individual hyperbolic echoes (Fig. 6) that approach the IIB-2 character of Damuth (1975) scheme. The origin of this echo character is said to be varied; bottom current and gravity-driven processes are postulated as possible formative processes, with setting being an important consideration. In the case presented by Damuth (1975) IIB-2 echoes are located adjacent to levees and distributary channels of the Amazon cone. However; more consolidated gravity controlled flows and mass movements may also result in type IIB-2 echoes being recorded from the respective deposits.

The floor of the Ariel Graben (Ch in Figs. 3, 4, and 5) has a varied echo character. In the west it is rough, with small overlapping hyperbolae (IIIC of Damuth 1975) showing evidence of erosional/depositional bedforms. Such bedforms from other basins have been ascribed to erosion in the bottom boundary layer (Flood 1980) and syndeposition (Tucholke 1979) related to bottom water circulation or gravity driven processes (Damuth 1975) depending on the setting.

The southern flank of the Ariel Graben is rugged, dominated by large hyperbolae. Such a strongly reflective, hyperbolic echo character typifies basement highs or outcrop (Damuth and Hayes 1977; Damuth 1980; Lee et al. 2002). In this case, the lower northern flank of the Dana Plateau is cropping out due to an overall lack of sediment deposition on the southern flank. As shown in Fig. 6 (profile E—E'), ponds of sediment (discontinuous sub-parallel reflectors) are present in troughs and depressions of the southern flank. This suggests a sediment starved environment on the southern flank of the Ariel Graben, and implies differential deposition within the study area.

Interpretation of bathymetric and 3.5 kHz data

The development of a crude plastered sediment drift in the west (on the northern flank) gives way to soft sediment deformation fields in the east of the northern flank of the Ariel Graben. This demonstrates changes in the depositional/erosional setting from west to east through the Ariel Graben along the northern flank. The plastered drifts are typical of depositional features associated with bottom water current circulation (Stow et al. 1996), yet the transition to the field of undulations is atypical and requires that others factors be involved in their formation.

The presence of these undulations could be explained by several processes including contour current/seafloor

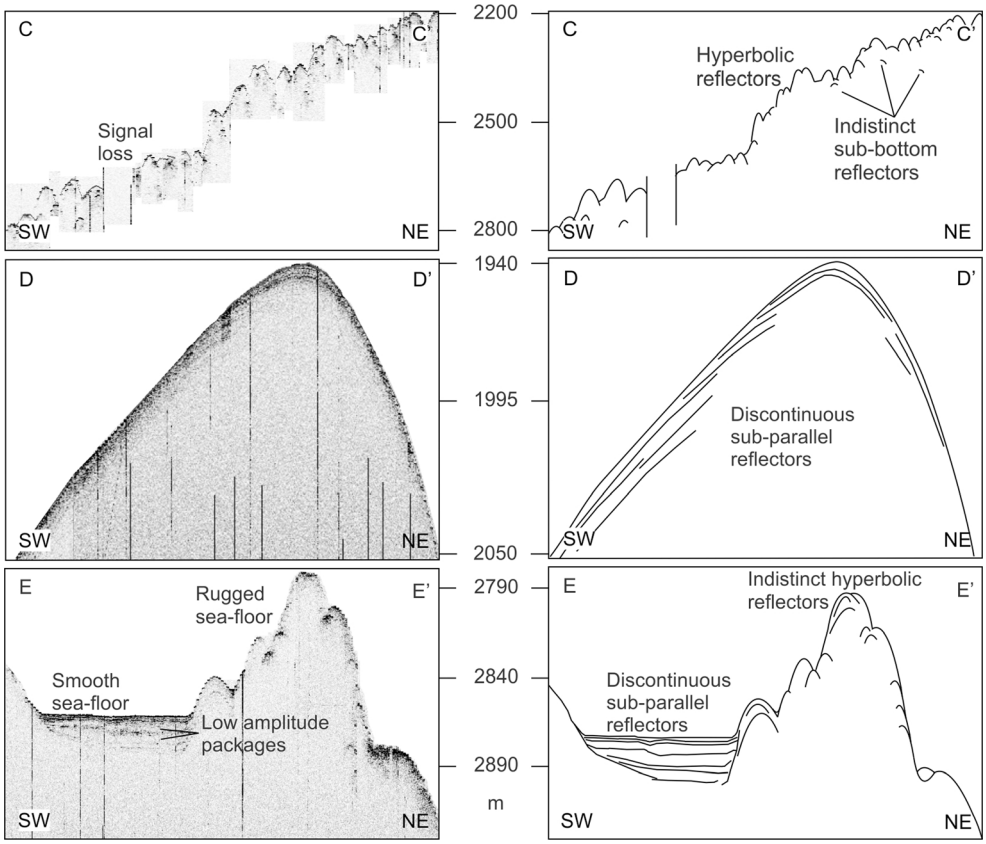

Fig. 6 Seismic character of profiles C—C', D—D', and E—E' (see Fig. 2, Box c, and Fig. 5 for location). Undulating sea floor is associated with hyperbolic echoes with indistinct sub-bottom returns. This is in contrast to the discontinuous sub-parallel reflectors of profile D—D', which is associated with smooth sea floor. On the southern flank of the Ariel Graben, hyperbolic echoes are similarly associated with rugged seafloor (Bs in Fig. 5), while horizontal, discontinuous sub-parallel echoes are evident in troughs adjacent to the rugged sea floor

interactions, turbidity current activity and mass-wasting/soft sediment deformation. Although the undulation dimensions are similar to features created by turbidity currents (see Table 2 for a comparison). In the setting presented here, the formative process associated with IIB-2 echoes is potentially related to deposition by turbidity currents. However, the undulation field is not associated with any deep sea canyon/channel/fan system. The nearest continental shelf that could shed sediment directly to the Ariel Graben is 380 km to the west. Apart from being sediment starved (Green 2009; Flemming 1980), this margin is separated from the Ariel Graben by the Central Terrace, disrupting the pathway of sediment by turbidity current. The Mozambique Ridge is obviously a feature which could play host to turbidity currents, however, in the setting of the Ariel Graben this is unlikely. There is no suitable staging area/source, directly to the north of the Ariel Graben, for the generation of turbidity driven flows. Hence, given the location of the undulation field of this study, deposits associated with turbidity currents are highly improbable.

Furthermore, from a morphological perspective, the character of the undulations is atypical of the surface expression of turbidites (Faugères et al. 2002; Wynn and Stow 2002). The wave-form (i.e., the general morphology of the undulations) dimensions of the undulations are larger in the upslope and downslope areas, decreasing in dimension toward the middle of the flank as opposed to the general decrease in wave dimension downslope (i.e., with distance from the source) expected of turbidity current-fed bedforms.

Table 1 Length and gradient characteristics of undulations

ID	Upslope limb (m)	Downslope limb (m)	Upslope limb (°)	Downslope limb (°)
1	550	650	1.66	−3.88
2	500	550	0.86	−5.64
3	400	600	2.81	−3.17
4	500	700	0.54	−3.15
5	400	600	2.11	−4.66
6	400	600	1.71	−2.80
7	400	450	0.65	−4.25
8	200	450	0.86	−5.09
9	200	400	1.18	−4.62
10	300	300	1.79	−3.28
11	300	400	0.41	−3.98
12	150	350	4.21	−5.59
13	200	350	0.26	−2.87
14	200	350	0.16	−3.15
15	200	800	3.04	−3.48
16	200	400	2.26	−5.46
17	200	750	1.78	−5.84
Average	323.53	511.76	1.55	−3.80

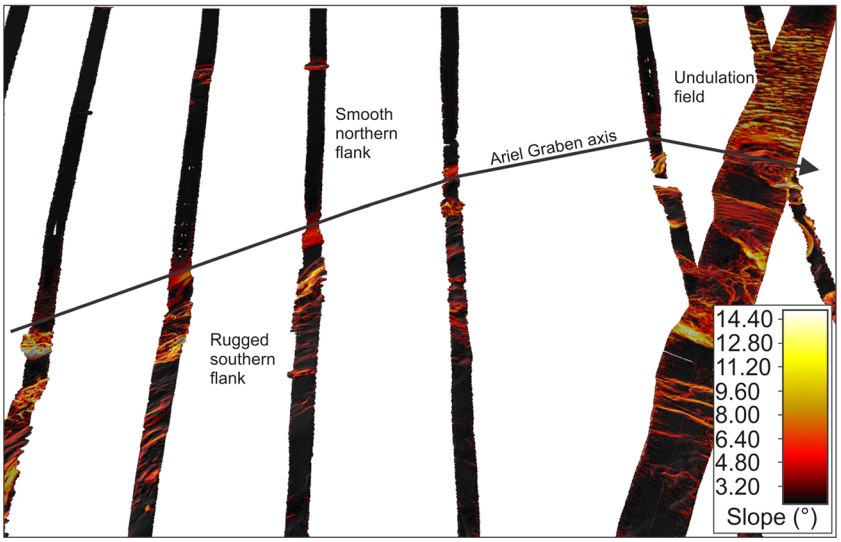

Fig. 7 3D perspective view slope map for the Ariel Graben looking south to north from the Dana plateau across the Ariel Graben. The strips of data reflect the slope of the seafloor as calculated from the bathymetry data from the same area. Note the difference in slope and relief between the northern and southern flanks of the Ariel Graben. The northern flank is relatively uniform, the exception being the undulations to the east which exhibit regular variance in gradient over short distances. In contrast, the southern flank exhibits varied gradients throughout the study area reflecting an irregular seafloor relief. The change in the orientation of the Ariel Graben (*from west to east*) is shown by the black arrow

With regards the genesis of sediment waves by bottom current interaction, the dimensions of the wave-forms observed in this study are similar to those of fine-grained bottom sediment waves (cf. Wynn and Stow 2002; Table 2 this study). Such fine-grained bottom sediment waves are found in sediment drift environments on the basin floor, lower slope and rise. At odds with this interpretation are the general orientations of the wave-form crests themselves. Typically, the crests of fine-grained bottom current sediment wave systems are oblique to the slope, or perpendicular to the flow direction of the current, with evidence of upslope and up-current migration of bedforms. In this study, the crests are parallel/subparallel to the maximum slope, orientated west–east; ~90° to the expected orientation (north–south) had they been directly developed by a current flowing west to east through the graben. As with a turbidity current-induced setting, the decrease then increase of the wave-form dimensions is in contrast to that of a bottom current sediment wave setting that generally produces decreasing wave-form dimensions with increased transport distance (Faugères et al. 2002; Wynn and Stow 2002).

The final alternative of downslope creep appears to be a viable option for the genesis of these features. There has been much discussion concerning the distinction between current generated sediment waves and undulations generated by creep/soft sediment deformation (Dillon et al. 1993; Gardner et al. 1999; Holbrook 2001; Lee and Chough 2001; Holbrook et al. 2002; Lee et al. 2002; Trincardi et al. 2004; Schwehr et al. 2007; Shillington et al. 2012). The debate stems from the similarities in bathymetry and seismic characteristics of these features. However, having excluded generation by bottom or turbidity current, soft sediment deformation is a likely formative process. In addition, the dimensions and characteristics of the seafloor undulations in this study (Table 2) are comparable to those associated with creep as described by Wynn and Stow (2002).

In keeping with the discussion in section Echo character contrasts and in the context of the bathymetry signatures discussed above, it is clear that the northern flank of the Ariel Graben is dominated by sediment cover, whereas the southern flank of the Ariel Graben exhibits basement control on sedimentation in a sediment starved setting with ponds of sediment filling low lying areas amidst the rugged bathymetry of the Dana Plateau's northern flank. The local outcrop of basement is likely to increase turbulence and promote the resuspension and redistribution of sediment rather than deposition. The net result is preferential deposition on the northern, rather than southern flank of the Ariel Graben. The resultant uneven depositional regime is at odds with the uniform distribution of sediment thicknesses attributed to pelagic deposition. Preferential drift deposition on the northern flank of the Ariel Graben is thus the likely driver of *downslope creep* here.

Significance of creep

Seafloor undulations generated by soft sediment deformation are often related to seismic activity. Examples from the Adriatic and Californian continental slopes describe such occurrences of seismically induced soft sediment deformation. However, such settings are far removed from the deep Ariel Graben of the Mozambique Ridge. The former two regions have recent and sustained seismic histories accounting for

Table 2 Summary of characteristics for different types of sediment waves, and also soft sediment deformation features (modified after Wynn and Stow 2002)

Wave-formingprocess	Turbidity current	Turbidity current	Bottom current	Bottom current	Soft sediment deformation (e.g. creep folds)	This study
Sediment grain Size	Fine-grained (mud and silt dominated)	Coarse-grained (sand and gravel dominated)	Fine-grained (mud and silt dominated)	Coarse-grained (sand and gravel dominated)	Varied: usually fine-grained (mud/silt dominated)	Unknown: presumed fine-grained
Environment	Channel levees, continental slope/rise	Canyons, channels and canyon/channel mouths	Sediment drifts on basin floor/lower slope/rise	Topographic ridges, continental slopes, b-c passages	Varied: potentially any submarine slope	Ariel Graben northern flank
Wavelength	Up to 7 km	Usually up to 1 km, rarely larger	Up to 10 km	Up to 200 m	Up to 10 km	600 m – 1.2 km
Wave height	Up to 80 m	Up to 10 m	Up to 150 m	A few metres	Up to 100 m	35–70 m
Key features	Usually on slopes of 0.1 to 0.7° Wave dimensions progressively decrease downslope Wave asymmetry usually decreases downslope Crests are roughly parallel to regional slope	Crests aligned perpendicular to flow direction Can show decrease in dimensions at channel margin Morphology is often irregular/disrupted Migration direction variable	Wave dimensions decrease near edge of wave field Wave symmetry decreases near edge of wave field Waves on slopes are aligned oblique to slope Most waves on slopes migrate upcurrent and upslope Crests are straight or slightly sinuous	Can occur as straight waves or barchans Both types aligned perpendicular to flow Barchans common where sediment supply is poor, migration is upcurrent Ripple patterns show peak flow near barchan crest	Most common on slopes of >2° Orientated perpendicular to maximum slope Do not show true lateral migration Usually show broard crests and narrow troughs Typically random scatter of dimensions	Orientated perpendicular to maximum slope Usually show board crests and narrow troughs Dimensions increase toward the edges, up and down slope.
Key examples	Monterey Fan levees (Normark et al. 1980) Bounty Channel levees (Carter et al. 1990) Toyama Channel levees (Nakajima and Satoh 2001) Var Fan levees (Migeon et al. 2000, 2001) Canary Islands slopes (Wynn et al. 2000a, b)	Var Canyon (Malinverno et al. 1988) Stromboli Canyon (Kidd et al. 1998) Valencia Channel mouth (Morris et al. 1998) Canary Islands (Wynn et al. 2000a) Laurentian Fan (Piper et al. 1985)	Argentine Basin (Flood et al. 1993) Rockall Trough (Howe 1996) Blake-Bahama Ridge (Flood 1994) Gardar Drift (Manley and Caress 1994) Falkland Trough (Cunningham and Barker 1996)	NW European slope (Kenyon 1986) Iceland-Faroe Ridge (Dorn and Werner 1993) Carnegie Ridge (Lonsdale and Malfait 1974) Gulf of Cadiz (Kenyon and Belderson 1973) Various sites (Lonsdale and Speiss 1977)	South Korea Plateau (Lee and Chough 2001) Beaufort Sea (Hill et al. 1982) Tingin Fjord (Syvitski et al. 1987) Landes Marginal Plateau (Kenyon et al. 1978) New England slope (O'Leary and Laine 1996)	

extensive soft sediment deformation fields (cf. Dengler et al. 1993; Tinti et al. 1995), whereas the Mozambique Ridge is comparatively stable (Leinweber and Jokat 2012). Recent findings suggest that there may be some tectonic activity associated with the southward propagation of the East African Rift System (Saria et al. 2014; Wiles et al. 2014). However, seismically induced deformation seems unlikely at this location as the soft sediment deformation is restricted to a specific area within the region rather than a wide-spread occurrence in line with seismically-induced deformation fields. High sedimentation rates, storm waves, and biological processes may also induce downslope movements through the increase of applied shear stress or reduction of the critical shear strength of sediments (Stow et al. 1996). At the depth of the undulations, storm waves are not considered, while biological activity is an unknown variable. A high sedimentation rate is therefore suggested as the most prominent factor in this instance, likely delivered by deep water bottom-interacting currents in the area.

Sediment redistribution via the Agulhas current or NADW?

In the northernmost Natal Valley, sediment redistribution at depths of between 400 and 1500 m on the Central Terrace, Limpopo Cone and adjacent continental shelf has been attributed to action of the Agulhas Current (Flemming and Hay 1988; Martin 1981a, 1981b; Preu et al. 2011). However, it is unlikely that the Agulhas Current at 27°S is as deep seated as it is to the south (32°S), where it reaches depths of 2500 m (Bang and Pearce 1976; Dingle et al. 1987, Beal and Bryden 1997; Donohue and Toole 2003). We attribute this to three reasons. Firstly, in this source region the Agulhas Current is still forming from the amalgamation of eddies from the north and east (Preu et al. 2011). Secondly, the Central Terrace lies in ca. 1500 m of water, so a deeper extension of the current to 2500 m is not possible. Thirdly, the observation by previous authors of a northerly flowing NADW in the west and a southerly flowing NADW in the east of the Natal Valley implies recirculation of this current system whereby NADW passes beneath the Agulhas Current at a deeper level. On this basis we consider the alternative hypothesis, bottom current activity and sediment re-organisation by the NADW.

Oceanographic constraints to potential NADW flow and a revised pathway

As a deep western boundary current plastered up against the east coast of South Africa by the Coriolis Effect, it is unlikely that its northward passage would be impeded until obstacles to that flow are encountered (Dingle et al. 1987; van Aken et al. 2004; Martínez-Méndez et al. 2008; McDonagh et al. 2008). The shoaling of the northern Natal Valley provides the necessary bathymetric restriction to change the pathway of the NADW. However this restriction within the known depth range of NADW is gradual and asymmetrical. The northern Natal Valley does not terminate in a horseshoe between 2000–3500 m (Fig. 8), but rather the Tugela cone and Central Terrace (fronted by the Naude' Ridge) provide initial restrictions from the west and northwest respectively (Fig. 8). These restrictions would force the NADW to shift from its original north northeast flow direction towards the northeast. The 2000 m isobath marks the shallow edge of the central terrace, and consequently the northward limit of NADW flow in the northern Natal Valley. Continuing to the northeast, the 2000 m isobaths of the Central Terrace merges with the top of the Ariel Graben's northern flank (Figs. 2 and 8). The Dana Plateau, located south east of the Central Terrace, rises to a minimum depth of 1795 m and consequently restricts the direct eastward flow of NADW into the Mozambique Basin (Fig. 8). The Dana Plateau thus offers a potential point divergence for NADW flow whereby a portion of the water mass can continue northeast into the Ariel Graben, while the remainder recirculates southward along the eastern margin of the Natal Valley.

Once the NADW enters the Ariel Graben its passage is likely defined by the graben long-axis; the orientation of which is not constant. From west to east the axis migrates in a clockwise manner, not confined to the orientation of the saddle axis. The average gradient of the graben flanks, particularly the northern flank, typically increases from west to east with the steepest gradient found where the saddle axis changes direction to the east (Fig. 7). It is in the east that the maximum axis curvature takes place and it is here that the upper portion of the NADW is likely to over-spill on to the northern flank, effectively over-shooting the bend in the graben axis. This over-spilling results in reduced velocity, and deposition of suspended load on the northern flank. Coriolis Effect is likely to also play a role. Deflection to the left (north in this case) further promotes preferential deposition of the northern flank of the Ariel Graben thereby compounding the result of over-spilling in the region of undulations. Such rapid sedimentation is said elevate pore pressure, and create weak planes within the deposited sediments (Shillington et al. 2012). Subsequent slow gravity-driven downslope motion and deformation generates the region of seafloor undulations on the northern flank of the Ariel Graben. Hence, this area represents an over-steepened plastered drift, developed in response to over-spilling of NADW in the Ariel Graben, the failure of which is manifest as seafloor undulations generated by down slope creep (Fig. 8).

The relevance of a revised deep water pathway

The complex macrotopography of the southwest Indian Ocean (SWIO), as demonstrated by Dingle et al. (1987), van Aken et al. (2004) and Casal et al. (2006), represents a significant

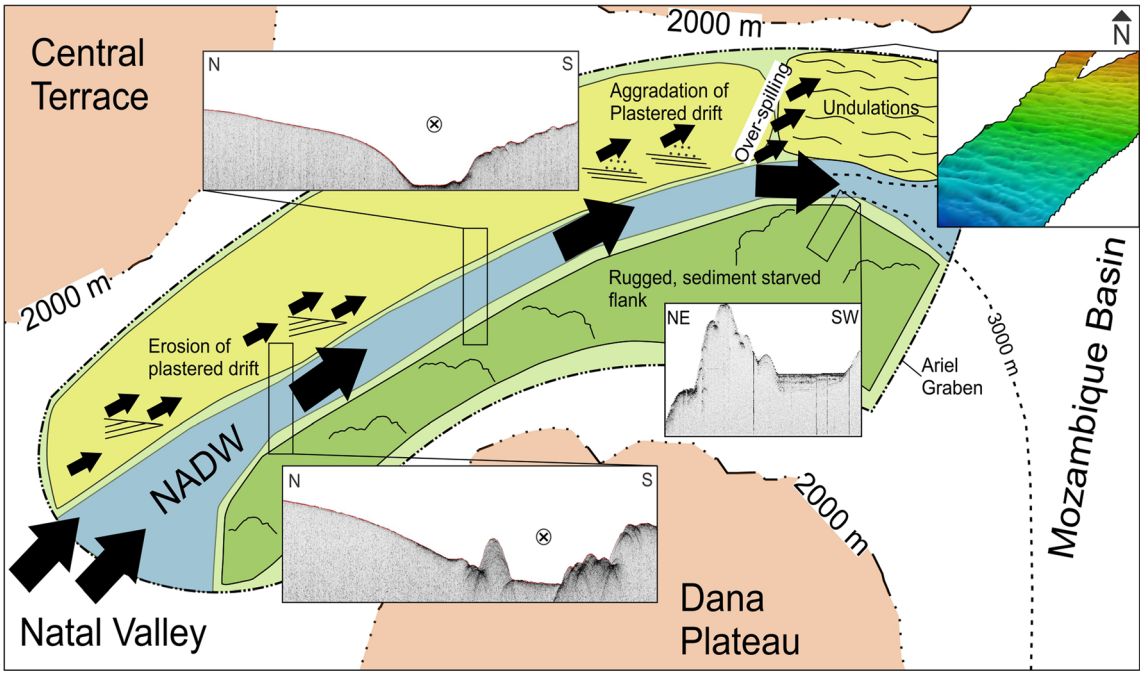

Fig. 8 Schematic of the study area (refer to Figs. 1 and 2) illustrating the proposed NADW pathway through the Ariel Graben. Once the water mass has entered the Ariel Graben its passage is determined by the axis of the graben. Proximally northeast orientated, the graben axis changes to east–southeast towards the distal areas in the east

factor in the control of deep THC flow (Donohue and Toole 2003). In this study, a previously unrecognised northern-most pathway for deep water exchange between the Natal Valley and the Mozambique Basin at 28°S is proposed (Fig. 9). The recognition of this pathway means the Natal Valley system and its effect on the SWIO region should be re-evaluated as the THC system and global climate are strongly linked (Martin 1981b; Martin 1987; Flemming and Hay 1988; Winter and Martin 1990; Martínez-méndez et al. 2008; Blome et al. 2012; Li et al. 2013; Menary and Scaife 2014).

With respect to NADW circulation interglacial periods typically see increased flow of NADW, while glacial periods are associated with reduced flow (Ben-Avraham et al. 1994; Alley et al. 1999; Rutberg et al. 2000). Increased flow, especially the proposed northern incursion of NADW, has implications for the ocean basins in which this water body is found, affecting deep water exchange between sub-basins within the SWIO (Fig. 9). The forcing of this deep water mass into rugged regions of shoaling bathymetry of the northern Natal Valley and Mozambique Ridge has the potential to increase upwelling in these regions, resulting in increased diapycnal mixing between water masses (Polzin et al. 1997).

As long-lived CO_2 sinks, such diapycnal mixing could be of ecological and climatological significance. It is suggested that CO_2 flushing from deep water masses is a step-wise process that includes elevated nutrient supply to the mid-depths, subsequently resulting rapid rage expansion of species, increased productivity and CO_2 sequestration within the mid-Ocean (Galbraith et al. 2007; Henry et al. 2014). These have important ramifications for the east coast of Africa's future fishery potentials.

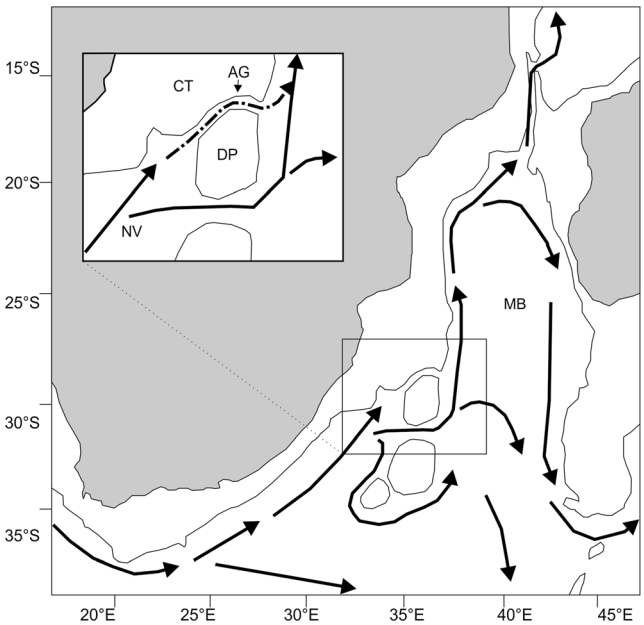

Fig. 9 The postulated passage of deep water (2000–3000 m), in this case NADW, through the SWIO is shown by black arrows, after van Aken et al. (2004). The 2000 m isobaths are shown for reference by the solid black line. The inset shows the study area, where the Ariel Graben creates a saddle across the Mozambique Ridge. The suggested NADW pathway across this saddle, through the Ariel Graben, is illustrated by the black dot-dash line. Abbreviations in insert: *CT* Central Terrace, *AG* Ariel Graben, *DP* Dana Plateau, *NV* Natal Valley

Conclusion

The Ariel Graben creates a deep west to east saddle across the Mozambique Ridge at ca. 28°S. This deep saddle in the Mozambique Ridge provides the potential for deep water exchange between the northern Natal Valley, and Mozambique Basin. A west to east change in character in the Ariel Graben is recorded in the sub-surface and expressed in the morphology of the seafloor and linked to deep water sediment trasnport. Evidence of this transport is manifest as crudely developed plastered drifts in the west and a field soft sediment deformation, of limited extent, in the east of the study area. Here current flow stripping due to increased curvature of the graben axis, results in preferential deposition of suspended load in accordance of reduced current velocity in an area of limited accommodation space. This results in an over-steepened plastered drift. Deposited sediments overcome the necessary shear stresses, resulting in soft sediment deformation in the form of down-slope growth faulting (creep) and generation of undulating seafloor morphology. The observed seafloor and subseafloor characteristics are considered to be associated with a newly postulated NADW passage through the Ariel Graben, as opposed to influence by deep-reaching Agulhas Current activity.

Acknowledgments We wish to thank the BMBF (Bundesministerium fur Bildung und Forschung) for funding the scientific projects (contract numbers 03G0183A, 03G0730A). The crews of RV Sonne (AISTEK II) and RV Pelagia (AISTEK III) are acknowledged for their excellent support and expertise in the data acquisition phases. The financial assistance of the National Research Foundation (Innovation Scholarship) (83799) towards this research is hereby acknowledged. Opinions expressed and conclusions arrived at, are those of the authors and are not necessarily to be attributed to the DAAD-NRF. Prof. Dr. BW Flemming and Dr. AK Martin are thanked for their welcomed reviews of the initial manuscript. Their input added greatly to the revised manuscript.

References

Alley RB, Clark PU, Keigwin LD, Webb RS (1999) Making sense of millennial-scale climate change. In: Clark PU, Webb RS, Keigwin LD (eds) Mechanisms of Global Climate Change at Millennial Time Scales. AGU Geophys Monogr 112:385–494

Bang ND, Pearce AF (1976) Large-scale circulation of surface water of the south Indian Ocean. In: Heydorn AEF (ed) Ecology of the Agulhas current region–an assessment of biological responses to environmental parameters in the south–west Indian Ocean. Proceedings of the marine freshwater conference, port Elizabeth. CSIR, Pretoria, pp 4–10

Beal LM, Bryden HL (1997) Observations of an Agulhas undercurrent. Deep-Sea Res I 44:1715–1724. doi:10.1016/S0967-0637(97)00033-2

Beal LM, Bryden HL (1999) The velocity and vorticity structure of the Agulhas current at 32° S. J Geophys Res 104(C3):5151–5176

Ben-Avraham Z, Niemi TM, Hartnady CJH (1994) Mid-tertiary changes in deep ocean circulation patterns in the natal valley and Transkei basin, southwest Indian ocean. Earth Planet Sci Lett 121(3–4):639–646

Blome MW, Cohen AS, Tyron CA, Brooks JR (2012) The environmental context for the origins of modern human diversity: a synthesis of regional variability in African climate 150,000–30,000 years ago. J Hum Evol 62:563–592

Carter L, Carter RM, Nelson CS, Fulthorpe CS, Neil HL (1990) Evolution of Pliocene to recent abyssal sediment waves on Bounty Channel levees, New Zealand. Mar Geol 95:97–109

Casal TGD, Beal LM, Lumpkin R (2006) A North Atlantic deep-watereddy in the Agulhas Current system. Deep-Sea Res I 53:1718–1728

Cawthra HC, Neumann FH, Uken R, Smith AM, Guastella L, Yates AM (2012) Sedimentation on the narrow (8 km wide), oceanic current-influenced continental shelf off Durban, KwaZulu-Natal, South Africa. Mar Geol 323–325:107–122

Cunningham AP, Barker PF (1996) Evidence for westward-flowing Weddell Sea Deep Water in the Falkland Trough, western South Atlantic. Deep-Sea Res 43:643–654

Damuth JE (1975) Echo characters of the western equatorial Atlantic floor and its relationship to the dispersal and distribution of terrigenous sediments. Mar Geol 18:17–45

Damuth JE (1980) Use of high-frequency (3.5–12 kHz) echograms in the study of near- bottom sedimentation processes in the deep sea: a review. Mar Geol 38:51–75

Damuth JE, Hayes DE (1977) Echo character of the east Brazilian continental margin and its relationship to sedimentary processes. Mar Geol 24:73–95

de Ruijter WPM, Biastoch A, Drijfhout SS, Lutjeharms JRE, Matano RP, Pichevin T, van Leeuwen PJ, Weijer W (1999) Indian-Atlantic interocean exchange: dynamics, estimation and impact. J Geophys Res 104:20885–20910

de Ruijter WPM, Ridderinkhof H, Lutjeharms JRE, Schouten MW, Veth C (2002) Observations of the flow in the Mozambique channel. Geophys Res Lett 29(10):1401–1403

de Ruijter WPM, van Aken HM, Beier EJ, Lutjeharms JRE, Matano RP, Schouten MW (2003) Eddies and dipoles around south Madagascar: formation, pathways and large-scale impact. Deep-Sea Res I 51:383–400

Dengler L, Carver GA, McPherson R (1993) Sources of north coast seismicity. Calif Geol 45:40–53

Dillon WP, Lee MW, Fehlhaber K, Coleman DF (1993) Gashydrates on the Atlantic margin of the United States—controls on concentration. In Howell DG (ed) the future of energy gases. Geol Surv Prof Pap 1570:313–330

DiMarco SF, Chapman P, Nowlin WD Jr, Hacker P, Donohue K, Luther M, Johnson GC, Toole J (2002) Volume transport and property distributions of the Mozambique channel. Deep-Sea Res II: Top Stud Oceanogr 49(7–8):1481–1511

Dingle RV, Robson S (1985) Slumps, canyons and related features on the continental margin off East London, SE Africa (SW Indian Ocean). Mar Geol 67:37–54

Dingle RV, Goodlad SW, Martin AK (1978) Bathymetry and stratigraphy of the northern Natal Valley (SW Indian Ocean): a preliminary account. Mar Geol 28:89–106

Dingle RV, Birch GF, Bremner JM, De Decker RH, du Plessis A, Engelbrecht JC, Fincham MJ, Fitton T, Flemming BW, Goodlad SW, Gentle RI, Martin AK, Mills EG, Moir GJ, Parker RJ, Robson SH, Rogers J, Salmon DA, Siesser WG, Simpson ESW, Summerhayes CP, Westall F, Winter A, Woodborne MW (1987) Deep-sea sedimentary environments around southern Africa (SE-Atlantic & SW-Indian Oceans). Ann S Afr Mus 98:1–27

Donohue KA, Toole JM (2003) A near-synoptic survey of the Southwest Indian Ocean. Deep-Sea Res II 50:1893–1931

Donohue KA, Firing E, Beal L (2000) Comparison of three velocity sections of the Agulhas current and Agulhas undercurrent. J Geophys Res Oceans 105(C12):28585–28593

Dorn WU, Werner F (1993) The contour-current flow along the southern Iceland-Faeroe Ridge as documented by its bedforms and asymmetrical channel fillings. Sediment Geol 82:47–59

Faugères JC, Stow DAV, Imbert P, Viana A (1999) Seismic features diagnostic of contourite drifts. Mar Geol 162:1–38

Faugères JC, Gonthier E, Mulder T, Kenyon N, Cirac P, Griboulard R, Berné S, Lesuavé R (2002) Multi-process generated sediment waves on the Landes plateau (Bay of Biscay, North Atlantic). Mar Geol 182(3–4):279–302

Flemming BW (1980) Sand transport and bedform patterns on the continental shelf between Durban and Port Elizabeth (Southeast African Continental Margin). Sediment Geol 26:179–205

Flemming B, Hay R (1988) Sediment distribution and dynamics of the Natal continental shelf, in Coastal Ocean Studies off Natal, South Africa, Lecture Notes. In: Schumann EH (ed) Coastal estuarine stud, vol 26. Springer, Berlin, pp 47–80

Flood RD (1980) Deep-sea sedimentary morphology: modelling and interpretation of echo-sounding profiles. Mar Geol 38:77–92

Flood RD (1994) Abyssal bedforms as indicators of changing bottom current flow: Examples from the U.S. East Coast continental rise. Paleoceanography 9:1049–1060

Flood RD, Shor AN, Manley PD (1993) Morphology of abyssal mudwaves at Project MUDWAVES sites in the Argentine Basin. Deep-Sea Res 40:859–888

Galbraith ED, Jaccard SL, Pedersen TF, Sigman DM, Haug DH, Cook M, Southon JR, Francois R (2007) Carbon dioxide release from the North Pacific abyss during the last deglaciation. Nature 449:890–893

Gardner J, Prior D, Field M (1999) Humboldt Slide—a large shear dominated retrogressive slope failure. Mar Geol 154:323–338

Goodlad SW (1986) Tectonic and sedimentary history of the mid-Natal Valley (SW Indian Ocean). Joint Geological Survey/University of Cape Town. Mar Geosci Unit Bull 15:415

Green AN (2009) Sediment dynamics on the narrow, canyon-incised and current-swept shelf of the northern KwaZulu-Natal continental shelf, South Africa. Geo-Mar Lett 29:201–219

Green AN (2011a) Submarine canyons associated with alternating sediment starvation and shelf-edge wedge development: Northern KwaZulu-Natal continental margin, South Africa. Mar Geol 289: 114–126

Green AN (2011b) The late Cretaceous to Holocene sequence stratigraphy of a sheared passive upper continental margin, northern KwaZulu-Natal, South Africa. Mar Geol 289:17–28

Green AN, Uken R (2008) Submarine landsliding and canyon evolution on the northern KwaZulu-Natal continental shelf, South Africa, SW Indian Ocean. Mar Geol 254:152–170

Green AN, Goff JA, Uken R (2007) Geomorphological evidence for upslope canyon-forming processes on the northern KwaZulu-Natal shelf, South Africa. Geo-Mar Lett 27:399–409

Gutjahr M, Hoogakker BAA, Frank M, McCave IN (2010) Changes in North Atlantic Deep Water strength and bottom water masses during Marine Isotope Stage 3 (45–35 ka BP). Quat Sci Rev 29:2451–2461. doi:10.1016/j.quascirev.2010.02.024

Henry LA, Frank N, Hebbeln D, Wienberg C, Robinson L, de Flierdt T, Dahl M, Douarin M, Morrison CL, Correa ML, Rogers AD, Ruckelshausen M, Roberts JM (2014) Global ocean conveyor lowers extinction risk in the deep sea. Deep-Sea Res Part I: Oceanogr Res Pap 88:8–16

Hill PR, Moran KM, Blasco SM (1982) Creep deformation of slope sediments in the Canadian Beaufort Sea. Geo-Mar Lett 2:163–170

Holbrook W (2001) Seismic studies of the Blake Ridge: implications for hydrate distribution, methane expulsion, and free gas dynamics. In: Paull C, Dillon W (eds) Natural Gas Hydrates: Occurrence, Distribution, and Detection. American Geophysical Union, Geophysical Monograph 124:235–256

Holbrook W, Lizarralde D, Pecher I, Gorman A, Hackwith K, Hornbach M, Saffer D (2002) Escape of methane gas through sediment waves in a large methane hydrate province. Geology 30(5):467–470

Howe JA (1996) Turbidite and contourite sediment waves in the northern Rockall Trough, North Atlantic Ocean. Sedimentology 43:219–234

Jacobi RD (1982) Microphysiographie du Sud-Est de l'Atlantique Nord et ses conséquences pour la distribution des processus prés du fond marin et des faciès associés, vol 31. Bull Inst Geol Bassin Aquitaine, Bordeaux, pp 31–46

Jokat W (2006) Southeastern Atlantic and Southwestern Indian Ocean: reconstruction of the sedimentary and tectonic development since the cretaceous, AISTEK-II: Mozambique Ridge and Mozambique Basin. Report of the RV "Sonne" Cruise SO-183, Project AISTEK-II 20 May to 7 July 2005 reports on Polar and Marine Research. Alfred-Wegener-Institute for Polar and Marine Research, Bremerhaven, p 71

Jokat W (2009) The expedition of the research vessel "Pelagia" to the Natal Basin and the Mozambique Ridge in 2009 (Project AISTEK III). Alfred-Wegener- Institute for Polar and Marine Research, Bremerhaven, p 67

Kenyon NH (1986) Evidence from bedforms for a strong poleward current along the upper continental slope of NW Europe. Mar Geol 72:187–198

Kenyon NH, Belderson RH (1973) Bedforms of the Mediterranean undercurrent observed with sidescan sonar. Sediment Geol 9:77–99

Kenyon NH, Belderson RH, Stride AH (1978) Channels, canyons and slump folds on the continental slope between south-west Ireland and Spain. Oceanol Acta 1:369–380

Kidd RB, Lucchi RG, Gee M, Woodside JM (1998) Sedimentary processes in the Stromboli Canyon and Marsili Basin, SE Tyrrhenian Sea: results from sidescan sonar surveys. Geo-Mar Lett 18:146–154

Lee SH, Chough SK (2001) High-resolution (2–7 kHz) acoustic and geometric characters of submarine creep deposits in the South Korea Plateau, East Sea. Sedimentology 48:629–644

Lee HJ, Syvitski JPM, Parker G, Orange D, Locat J, Hutton EWH, Imran J (2002) Distinguishing sediment waves from slope failure deposits: field examples, including the "Humboldt Slide", and modelling results. Mar Geol 192:79–104

Leinweber VT, Jokat W (2011) Is there continental crust underneath the Northern Natal Valley and the Mozambique Coastal Plains? Geophys Res Lett 38:L14303

Leinweber VT, Jokat W (2012) The Jurassic history of the Africa-Antarctica Corridor - new constraints from magnetic data on the conjugate continental margins. Tectonophysics 530–531:87–101. doi:10.1016/j.tecto.2011.11.008

Li C, von Storch JS, Marotzke J (2013) Deep-ocean heat uptake and equilibrium climate response. Climate Dynam 40(5–6):1071–1086

Lonsdale P, Malfait B (1974) Abyssal dunes of foraminiferal sand on the Carnegie Ridge. GSA Bull 85:1697–1712

Lonsdale PF, Speiss FN (1977) Abyssal bedforms explored with a deeply towed instrument package. Mar Geol 23:57–75

Lutjeharms JRE (2006a) The Agulhas current. Springer, Berlin, p 329

Lutjeharms JRE (2006b) The coastal oceans of south-eastern Africa. In: Robinson AR, Brink KH (eds) The Sea, vol 14B. Harvard University Press, Cambridge, pp 783–834

Lutjeharms JRE (2007) Three decades of research on the greater Agulhas current. Ocean Sci 3(1):129–147

Maldonado A, Barnolas A, Bohoyo F, Galindo-Zaldívar J, Hernández-Molina J, Lobo F, Rodríguez-Fernández J, Somoza L, Tomás Vázquez J (2003) Contourite deposits in the central Scotia Sea: the importance of the Antarctic circumpolar current and the Weddell gyre flows. Palaeogeogr Palaeoclimatol Palaeoecol 198(1–2):187–221

Malinverno A, Ryan WBF, Auffret G, Pautot G (1998) Sonar images of the path of recent failure events on the continental margin off Nice, France. GSA Spec Pap 229:59–76

Manley PL, Caress DW (1994) Mudwaves on the Gardar sediment drift, NE Atlantic. Paleoceanography 9:973–988

Martin AK (1981a) The influence of the Agulhas current on the physiographic development of the northernmost Natal Valley (SW Indian ocean). Mar Geol 39:259–276

Martin AK (1981b) Evolution of the Agulhas current and its palaeoecological implications. S Afr J Sci 77:547–554

Martin AK (1987) A comparison of sedimentation rates in the Natal Valley, S.W. Indian Ocean, with modern sediment yields in east coast Rivers, Southern Africa. S Afr J Sci 83:716–724

Martin AK, Hartnady CJH (1986) Plate tectonic development of the south West Indian Ocean: A revised reconstruction of East Antarctica and Africa. J Geophys Res 91:4767–4786

Martínez-Méndez G, Zahn R, Hall IR, Pena LD, Cacho I (2008) 345,000-year-long multi-proxy records off South Africa document variable contributions of northern versus southern component water to the deep south Atlantic. Earth Planet Sci Lett 267(1–2):309–321

Masson DG, Watts AB, Gee MJR, Urgeles R, Mitchell NC, Le Bas TP, Canals M (2002) Slope failures on the flanks of the western Canary Islands. Earth Sci Rev 57(1–2):1–35. doi:10.1016/S0012-8252(01)00069-1

McDonagh EL, Bryden HL, King BA, Sanders RJ (2008) The circulation of the Indian Ocean at 32°S. Prog Oceanogr 79:20–36

Menary M, Scaife A (2014) Naturally forced multidecadal variability of the Atlantic meridional overturning circulation. Climate Dynam 42(5–6):1347–1362

Migeon S, Savoye B, Faugeres J-C (2000) Quaternary development of migrating sediment waves in the Var deep-sea fan: distribution, growth pattern, and implication for levee evolution. Sediment Geol 133:265–293

Migeon S, Savoye B, Zanella E, Mulder T, Faugeres J-C, Weber O (2001) Detailed seismic-reflection and sedimentary study of turbidite sediment waves on the Var Sedimentary Ridge (SE France): significance for sediment transport and deposition and for the mechanics of sediment-wave construction. Mar Pet Geol 18:179–208

Morris SA, Kenyon NH, Limonov AF, Alexander J (1998) Downstream changes of large-scale bedforms in turbidites around the Valencia channel mouth, north-west Mediterranean: implications for paleoflow reconstruction. Sedimentology 45:365–377

Nakajima T, Satoh M (2001) The formation of large mudwaves by turbidity currents on the levees of the Toyama deep-sea channel, Japan Sea. Sedimentology 48:435–463

Niemi TM, Ben-Avraham Z, Hartnady CJH, Reznikov M (2000) Post-Eocene seismic stratigraphy of the deep ocean basin adjacent to the southeast African continental margin: a record of geostrophic bottom current systems. Mar Geol 162(2–4):237–258

Normark WR, Hess GR, Stow DAV, Bowen AJ (1980) Sediment waves on the Monterey Fan levee: a preliminary physical interpretation. Mar Geol 37:1–18

O'Leary DWO, Laine E (1996) Proposed criteria for recognizing intrastratal deformation features in marine high resolution seismic reflection profiles. Geo-Mar Lett 16:305–312

Pearce AF (1977) Some features of the upper 500m of the Agulhas current. J Mar Res 35(4):731–753

Piper DJW, Shor AN, Farre JA, O'Connell S, Jacobi R (1985) Sediment slides and turbidity currents on the Laurentian Fan: sidescan sonar observations near the epicentre of the 1929 Grand Banks earthquake. Geology 13:538–541

Polzin KL, Toole JM, Ledwell JR, Schmitt RW (1997) Spatial variability of turbulent mixing in the abyssal ocean. Science 276:93–96

Preu B, Spieß V, Schwenk T, Schneider RR (2011) Evidence for current-controlled sedimentation along the southern Mozambique continental margin since Early Miocene times. Geo-Mar Lett 31(5–6):427–435. doi:10.1007/s00367-011-0238-y

Quartly GD, Srokosz MA (2004) Eddies in the southern Mozambique channel. Deep-Sea Res Part II: Top Stud Oceanogr 51(1–3):69–83

Raymo ME, Ruddiman WF, Shackleton NJ, Oppo DW (1990) Evolution of Atlantic-pacific gradients over the last 2.5 m.y. Earth Planet Sci Lett 97:353–368

Raymo ME, Oppo DW, Curry W (1997) The mid-Pleistocene climate transition: a deep sea carbon isotopic perspective. Paleoceanography 12:546–559

Rutberg RL, Hemming SR, Goldstein SL (2000) Reduced north Atlantic deep water flux to the glacial southern ocean inferred from neodymium isotope ratios. Nature 405:935–938

Saria E, Calais E, Stamps DS, Delvaux D, Hartnady CJH (2014) Present-day kinematics of the East African rift. J Geophys Res Solid Earth 119:3584–3600. doi:10.1002/2013JB010901

Schlüter P, Uenzelmann-Neben G (2008) Indications for bottom current activity since Eocene times: the climate and ocean gateway archive of the Transkei basin, South Africa. Global Planet Change 60:416–428

Schmieder F, von Dobeneck T, Bleil U (2000) The Mid-Pleistocene climate transition as documented in the deep South Atlantic ocean: initiation, interim state and terminal event. Earth Planet Sci Lett 179:539–549

Schwehr K, Driscoll N, Tauxe L (2007) Origin of continental margin morphology: Submarine-slide or downslope current-controlled bedforms, a rock magnetic approach. Mar Geol 240:19–41. doi:10.1016/j.margeo.2007.01.012

Shillington DJ, Seeber L, Sorlien CC, Steckler MS, Kurt H, Dondurur D, Çifçi G, İmren C, Cormier MH, McHugh CMG, Gürçay S, Poyraz D, Okay S, Atgın O, Diebold JB (2012) Evidence for widespread creep on the flanks of the Sea of Marmara transform basin from marine geophysical data. Geology 40(5):439–442

Srinivasan A, Garraffo Z, Iskandarani M (2009) Abyssal circulation in the Indian ocean from a resolution global hindcast. Deep-Sea Res I: Oceanogr Res Pap 56(11):1907–1926

Stow DAV, Mayall M (2000) Deep-water sedimentary systems: New models for the 21st century. Mar Pet Geol 17(2):125–135

Stow DAV, Reading HG, Collison JD (1996) Deep seas. In: Reading HG (ed) Sedimentary environments: processes, facies and stratigraphy. Blackwell Science, Oxford, pp 395–453

Stramma L, Lutjeharms JRE (1997) The flow field of the subtropical gyre of the south Indian ocean. J Geophys Res 102:5513–5530

Syvitski JPM, Burrell DC, Skei JM (1987) Fjords: Processes and Products. Springer Verlag, New York, p 379

Tinti S, Maramai A, Favali P (1995) The gargano promontory: an important Italian seismogenetic–tsunamigenic area. Mar Geol 122:227–241

Toole JM, Warren BA (1993) A hydrographic section across the subtropical South Indian Ocean. Deep-Sea Res I 40:1973–2019

Trincardi F, Cattaneo A, Correggiari A, Ridente D (2004) Evidence of soft sediment deformation, fluid escape, sediment failure and regional weak layers within the late quaternary mud deposits of the Adriatic Sea. Mar Geol 213(1–4):91–119

Tucholke BE (1979) Furrows and focuses echoes on the Blake outer ridge. Mar Geol 31:13–20

Ullgren JE, van Aken HM, Ridderinkhof H, de Ruijter WPM (2012) The hydrography of the Mozambique channel from six years of continuous temperature, salinity, and velocity observations. Deep-Sea Res I Oceanogr Res Pap 69:36–50

van Aken HM, Ridderinkhof H, de Ruijter WPM (2004) North Atlantic deep water in the south-western Indian ocean. Deep-Sea Res I 51:755–776

Wiles E, Green A, Watkeys M, Jokat W, Krocker R (2013) The evolution of the Tugela canyon and submarine fan: a complex interaction between margin erosion and bottom current sweeping, southwest Indian Ocean, South Africa. Mar Pet Geol 44:60–70

Wiles E, Green A, Watkeys M, Jokat W, Krocker R (2014) Anomalous seafloor mounds in the northern natal valley, southwest Indian Ocean: implications for the east African rift system. Tectonophysics 630:300–312. doi:10.1016/j.tecto.2014.05.030

Winter A, Martin, AK (1990) Late Quaternary history of the Agulhas Current. Paleoceanography 5(4):479–486

Wynn RB, Stow DAV (2002) Classification and characterisation of deep-water sediment waves. Mar Geol 192:7–22

Wynn RB, Masson DG, Stow DAV, Weaver PPE (2000a) Turbidity current sediment waves on the submarine slopes of the western Canary Islands. Mar Geol 163:185–198

Wynn RB, Weaver PPE, Ercilla G, Stow DAV, Masson DG (2000b) Sedimentary processes in the Selvage sediment-wave field, NE Atlantic: new insights into the formation of sediment waves by turbidity currents. Sedimentology 47:1181–1197